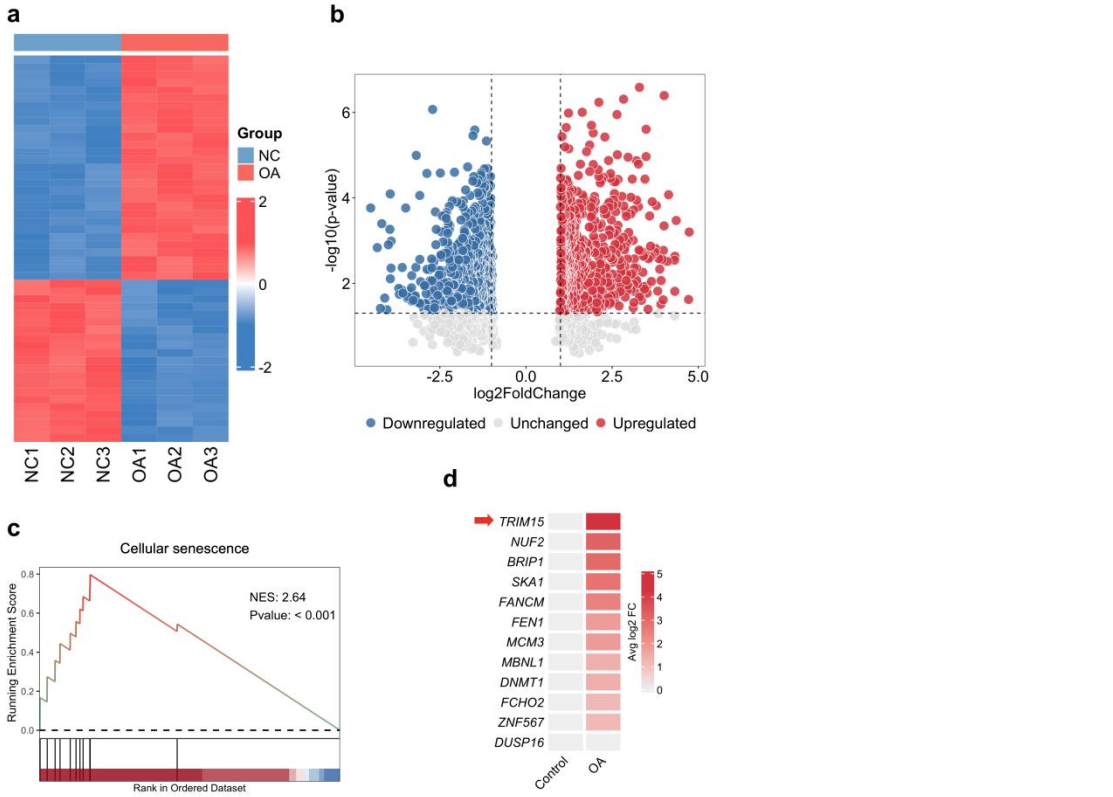

Supplementary Fig. 1. Transcriptomic identification of TRIM15 upregulation and senescence-associated signatures in osteoarthritic cartilage.

a, Heatmap showing the global expression pattern of differentially expressed genes in normal control (NC, n = 3) and osteoarthritic (OA, n = 3) human cartilage samples (GSE281609).

b, Volcano plot showing differentially expressed genes between NC and OA cartilage. Red dots indicate upregulated genes, blue dots indicate downregulated genes, and grey dots indicate genes without significant change.

c, Gene set enrichment analysis (GSEA) showing significant enrichment of the cellular senescence pathway in OA cartilage relative to NC cartilage. NES, normalized enrichment score.

d, Heatmap showing the expression of representative senescence-associated genes in NC and OA cartilage samples. TRIM15 is highlighted in red.

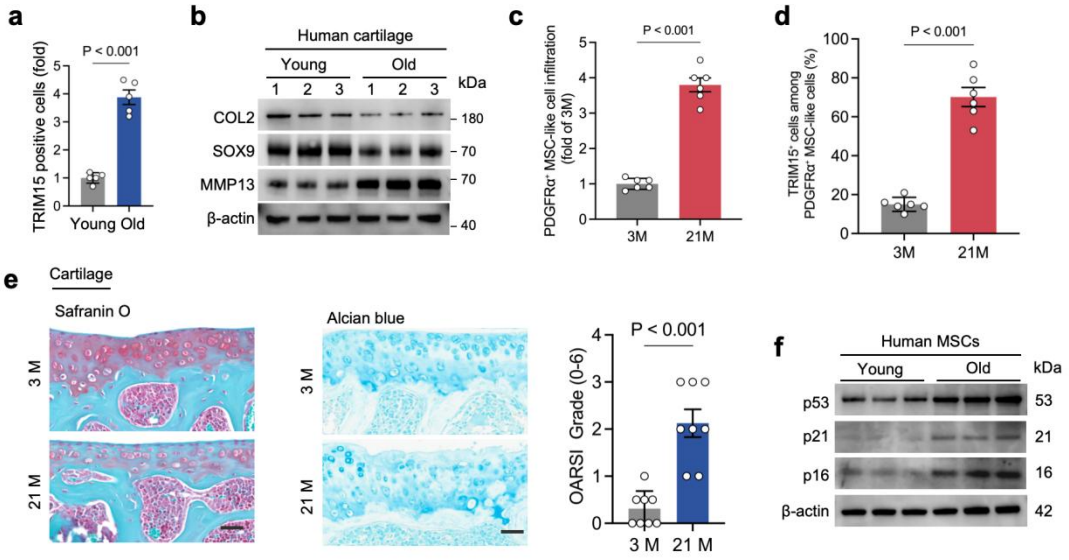

Supplementary Fig. 2. Additional validation of TRIM15 upregulation, cartilage degeneration, lesion-associated MSC-like cell accumulation and MSC senescence in aged joints.

a, Quantification of TRIM15-positive cells in human cartilage from young and old donors.

b, Immunoblot analysis of COL2, SOX9 and MMP13 protein expression in human cartilage samples from young and old donors. β-actin was used as the loading control.

c, Quantification of PDGFRα-positive MSC-like cell accumulation in cartilage-adjacent lesion regions of 3-month-old (3M) and 21-month-old (21M) mouse joints.

d, Quantification of TRIM15-positive cells among PDGFRα-positive MSC-like cells in 3M and 21M mouse joints.

e, Representative Safranin O and Alcian blue staining images of knee cartilage from 3M and 21M mice, with quantification of OARSI grade. Scale bars, 100 μm.

f, Immunoblot analysis of senescence-associated proteins p53, p21 and p16 in human MSCs from young and old donors. β-actin was used as the loading control.

Data are presented as mean ± s.d. (**a,c–d**).OARSI grades are presented as median with interquartile range and were analysed using a two-sided Mann–Whitney U-test. Each dot represents one biologically independent human donor (**a**) or mouse joint (**c–e**). P values were determined using two-sided unpaired Student's t-test.

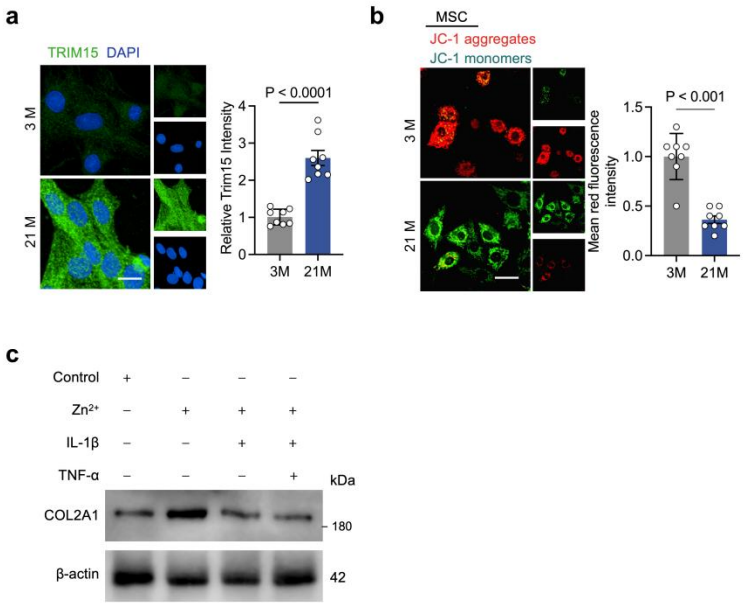

Supplementary Fig. 3 Additional validation of TRIM15 upregulation and mitochondrial dysfunction in aged MSCs, and zinc-responsive regulation in chondrocytes.

a, Representative immunofluorescence images and quantification of TRIM15 expression in MSCs isolated from 3-month-old (3M) and 21-month-old (21M) mice. Nuclei were counterstained with DAPI. Scale bars, 10 μm.

b, Representative JC-1 staining images and quantification of mitochondrial membrane potential in MSCs isolated from 3M and 21M mice. Red fluorescence indicates JC-1 aggregates and green fluorescence indicates JC-1 monomers. Scale bars, 10 μm.

c, Immunoblot analysis of COL2A1 protein expression in chondrocytes treated under the indicated conditions. β-actin was used as the loading control.

Data are presented as mean ± s.d. (**a,b**). Each dot represents one biologically independent sample. P values were determined using two-sided unpaired Student's t-test.

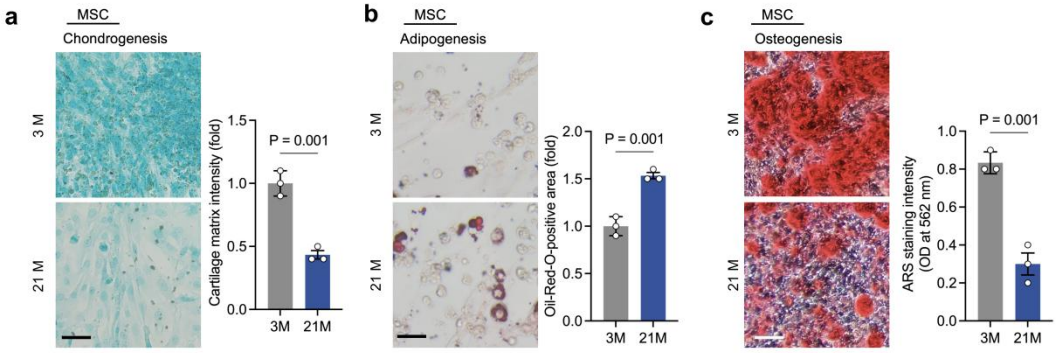

Supplementary Fig. 4. Tri-lineage differentiation assays of joint-derived MSCs from young and aged mice.

a, Representative Alcian blue staining images and quantification of chondrogenic differentiation in MSCs isolated from 3-month-old (3M) and 21-month-old (21M) mice.

b, Representative Oil Red O staining images and quantification of adipogenic differentiation in MSCs isolated from 3M and 21M mice.

c, Representative Alizarin Red S staining images and quantification of osteogenic differentiation in MSCs isolated from 3M and 21M mice.

Data are presented as mean ± s.d. (**a–c**). Each dot represents one biologically independent sample. P values were determined using two-sided unpaired Student's t-test. Scale bars, 50 μm.

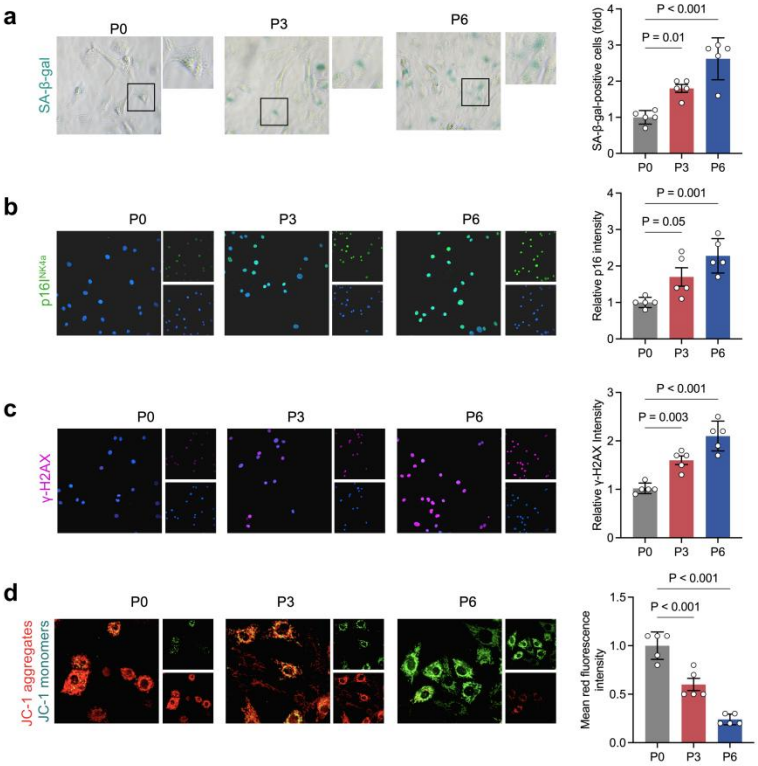

Supplementary Fig. 5. Validation of senescence-associated changes in serially passaged BMSCs.

a, Representative SA-β-gal staining images and quantification of SA-β-gal-positive cells in BMSCs at passages P0, P3 and P6.

b, Representative immunofluorescence images and quantification of $p16^{INK4a}$ expression in BMSCs at P0, P3 and P6. Nuclei were counterstained with DAPI.

c, Representative immunofluorescence images and quantification of γ-H2AX expression in BMSCs at P0, P3 and P6. Nuclei were counterstained with DAPI.

d, Representative JC-1 staining images and quantification of mitochondrial membrane potential in BMSCs at P0, P3 and P6. Red fluorescence indicates JC-1 aggregates, and green fluorescence indicates JC-1 monomers.

Data are presented as mean ± s.d. (a–d). Each dot represents one biologically independent sample. P values were determined using one-way ANOVA followed by Tukey's multiple-comparison test. Scale bars, 100 μm (a); 10 μm (b–d).

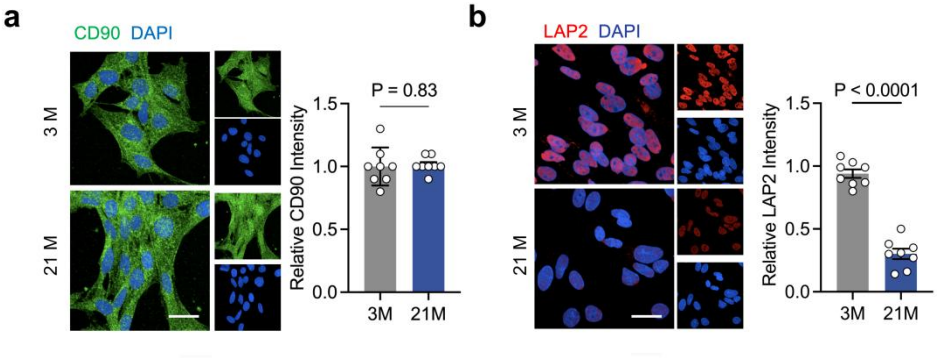

Supplementary Fig. 6. Validation of MSC identity and senescence-associated marker expression in young and aged mouse MSCs.

a, Representative immunofluorescence images and quantification of CD90 expression in MSCs isolated from 3-month-old (3M) and 21-month-old (21M) mice. Nuclei were counterstained with DAPI.

b, Representative immunofluorescence images and quantification of LAP2 expression in MSCs isolated from 3M and 21M mice. Nuclei were counterstained with DAPI.

Data are presented as mean ± s.d.(**a,b**). Each dot represents one biologically independent sample. P values were determined using two-sided unpaired Student's t-test. Scale bars, 10 μm.

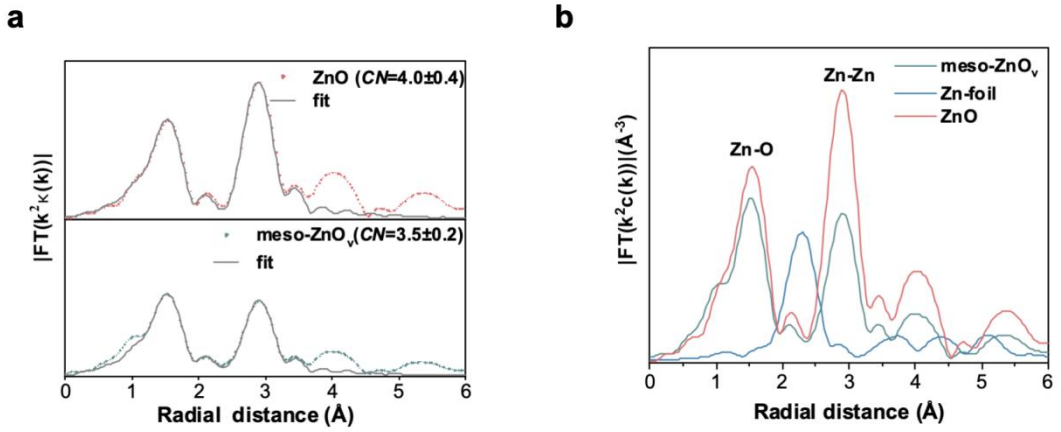

Supplementary Fig. 7. Zn K-edge EXAFS analysis of meso-ZnO_v.

a, Comparison of oxygen coordination number (CN) based on R-space Zn K-edge EXAFS fitting for ZnO and meso-ZnO_v. The reduced Zn–O coordination number in meso-ZnO_v is consistent with the presence of oxygen vacancies.

b, Fourier-transformed Zn K-edge EXAFS spectra of meso-ZnO_v, ZnO and Zn foil. The peaks corresponding to Zn–O and Zn–Zn coordination are indicated.

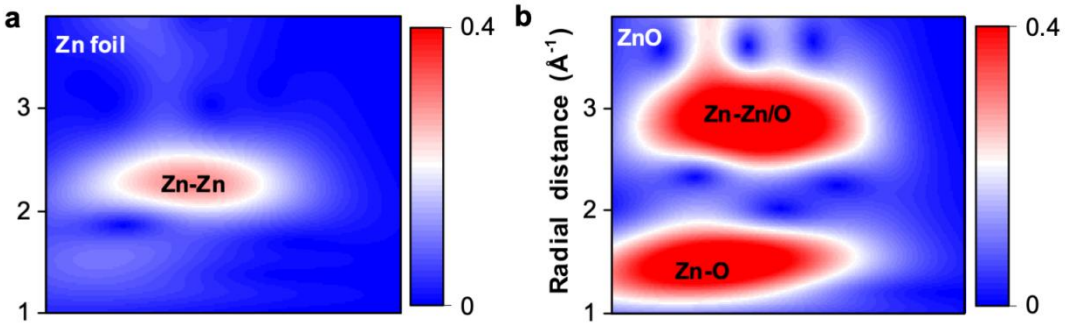

Supplementary Fig. 8. Wavelet transform plots for (a) Zn foil and (b) ZnO.

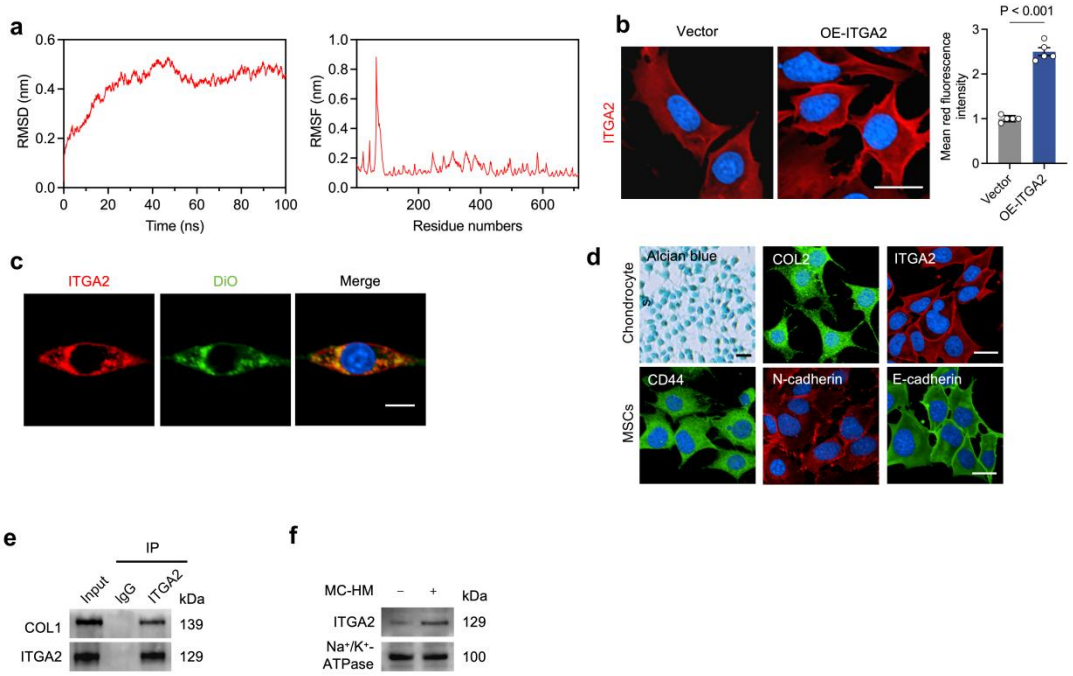

Supplementary Fig. 9. Validation of the ITGA2–COL1 interaction and characterization of membrane-source cells and hybrid membranes.

a, Root-mean-square deviation (RMSD) over 100 ns and residue-level root-mean-square fluctuation (RMSF) of the ITGA2–COL1 complex during molecular dynamics simulation.

b, Representative immunofluorescence images and quantification of ITGA2 expression in vector-control and ITGA2-overexpressing (OE-ITGA2) chondrocytes. Scale bars, 10 μm.

c, Representative images showing the colocalization of ITGA2 with the membrane dye DiO in OE-ITGA2 chondrocytes. Scale bars, 10 μm.

d, Representative Alcian blue staining and immunofluorescence images showing COL2 and ITGA2 in chondrocytes and CD44, N-cadherin and E-cadherin in MSCs used for membrane preparation. Scale bars, 10 μm.

e, Co-immunoprecipitation analysis of the association between ITGA2 and COL1, with input and IgG controls.

f, Immunoblot analysis of ITGA2 in MC-HM preparations. Na^+/K^+-ATPase served as a membrane loading control.

Data are presented as mean ± s.d. (**b**); each dot represents one biologically independent sample. Statistical significance was determined using a two-sided unpaired Student's t-test.

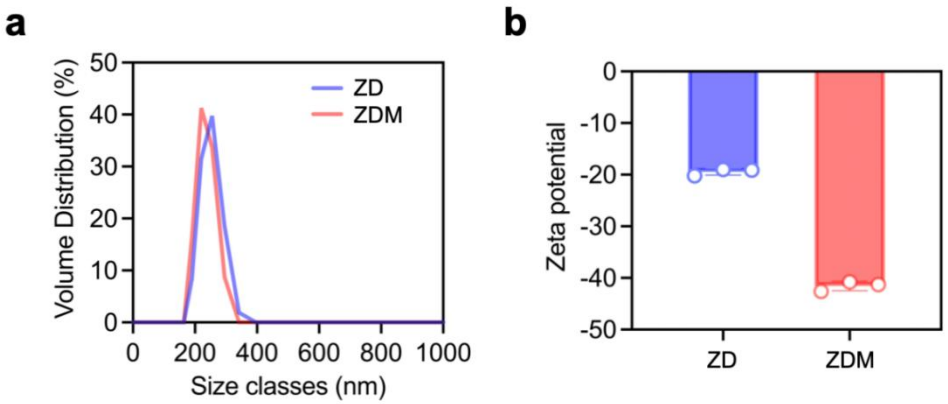

Supplementary Fig. 10. Hydrodynamic size and surface charge characterization of ZD and ZDM.

a, Dynamic light scattering analysis showing the hydrodynamic size distribution of ZD and ZDM.

b, Zeta potential measurements of ZD and ZDM, showing a more negative surface charge after hybrid membrane coating.

Data are presented as mean ± s.d. (**b**). Each dot represents one biologically independent sample.

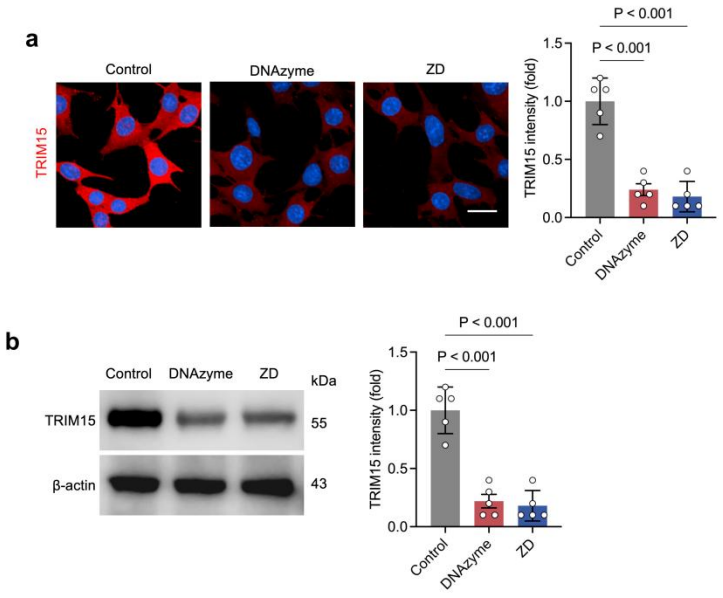

Supplementary Fig. 11. Validation of TRIM15 silencing by free DNAzyme and ZD.

a, Representative immunofluorescence images and quantification of TRIM15 expression in cells treated with vehicle (Control), free DNAzyme or ZD. Nuclei were counterstained with DAPI.

b, Immunoblot analysis and quantification of TRIM15 protein expression in cells treated with Control, free DNAzyme or ZD. β-actin was used as the loading control.

Data are presented as mean ± s.d. (**a**,**b**). Each dot represents one biologically independent sample. P values were determined using one-way ANOVA followed by Tukey's multiple-comparison test. Scale bars, 10 μm.

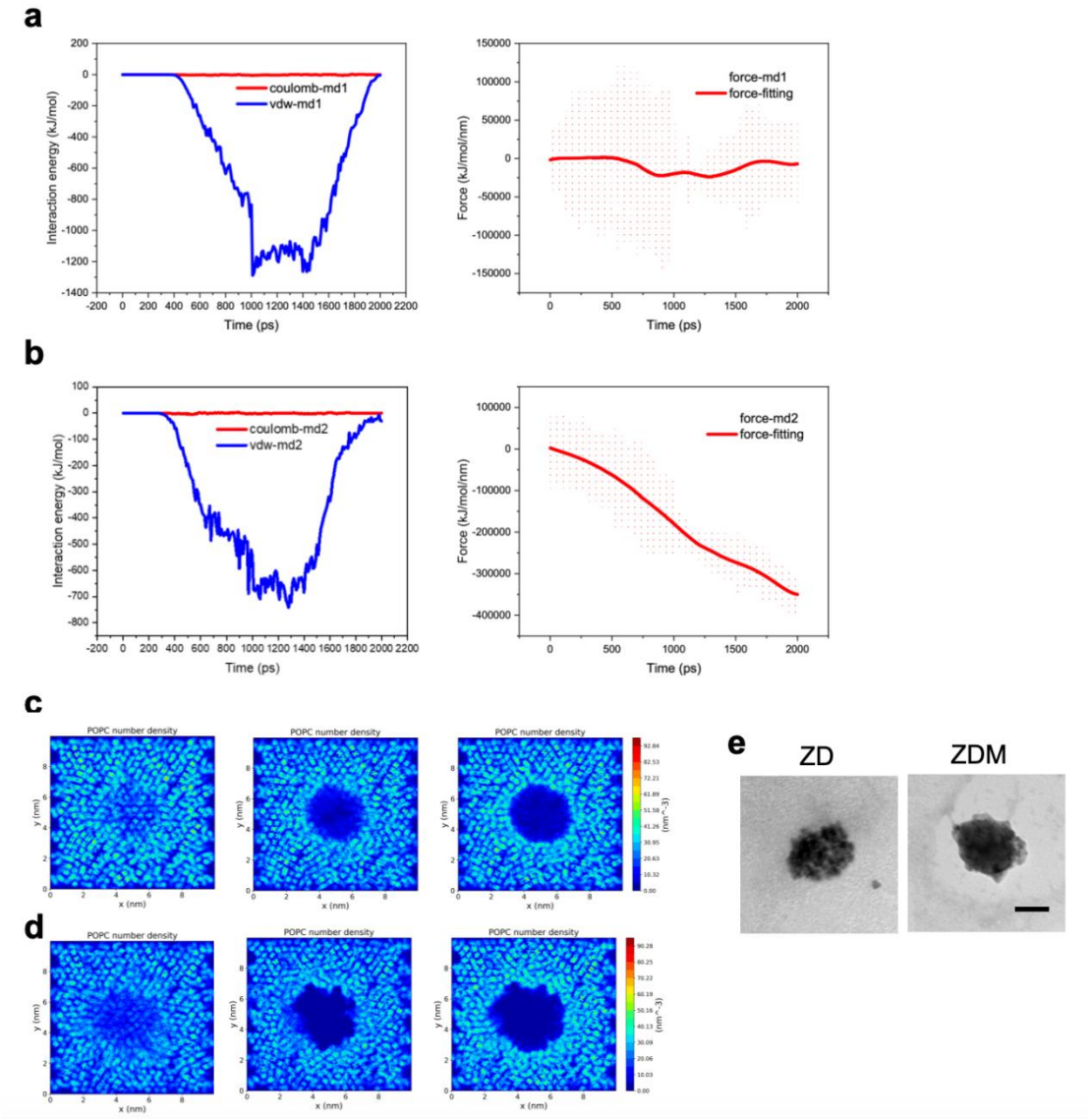

Supplementary Fig. 12. Molecular dynamics analysis of membrane interactions and morphological characterization of ZD and ZDM.

a,b, Time-dependent Coulombic and van der Waals interaction energies (left) and instantaneous force profiles with fitted curves (right) during the translocation of ZD (**a**) and ZDM (**b**) across the POPC phospholipid bilayer.

c,d, Representative POPC number-density maps showing the spatial redistribution of phospholipids during the translocation of ZD (**c**) and ZDM (**d**).

e, Representative TEM images of ZD and ZDM. ZDM exhibited a peripheral coating layer consistent with hybrid membrane encapsulation, which was absent from ZD. Scale bar, 100 nm.

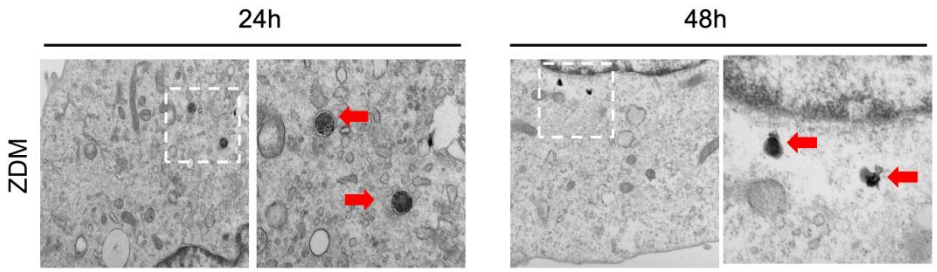

Supplementary Fig. 13. Intracellular degradation of ZDM visualized by transmission electron microscopy.

Representative transmission electron microscopy (TEM) images showing intracellular ZDM particles at 24 h and 48 h after incubation.

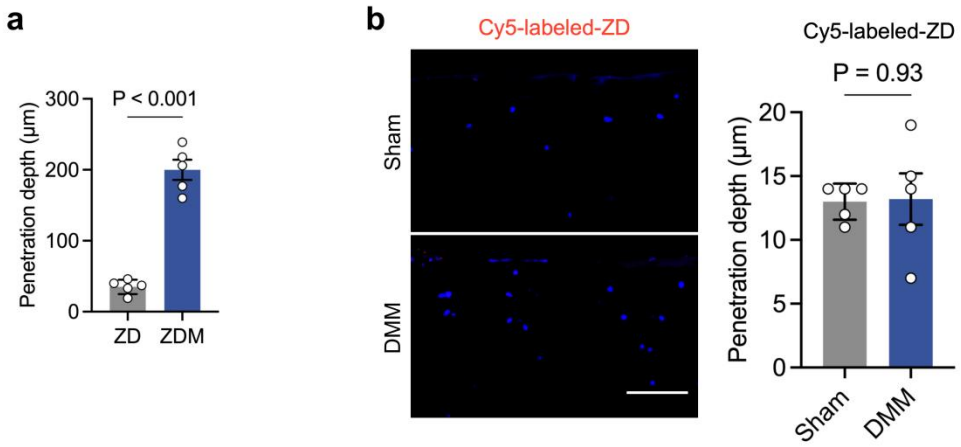

Supplementary Fig. 14. Quantification of cartilage penetration by ZDM and control analysis of Cy5-labelled ZD in vivo.

a, Quantification of cartilage penetration depth of ZD and ZDM in cartilage explants after incubation with Cy5-labelled nanoparticles.

b, Representative cryosection fluorescence images and quantification of penetration depth of Cy5-labelled ZD in sham and DMM mouse knee joints following intra-articular injection.

Data are presented as mean ± s.d. (**a,b**). Each dot represents one biologically independent sample. Scale bar, 100 μm.

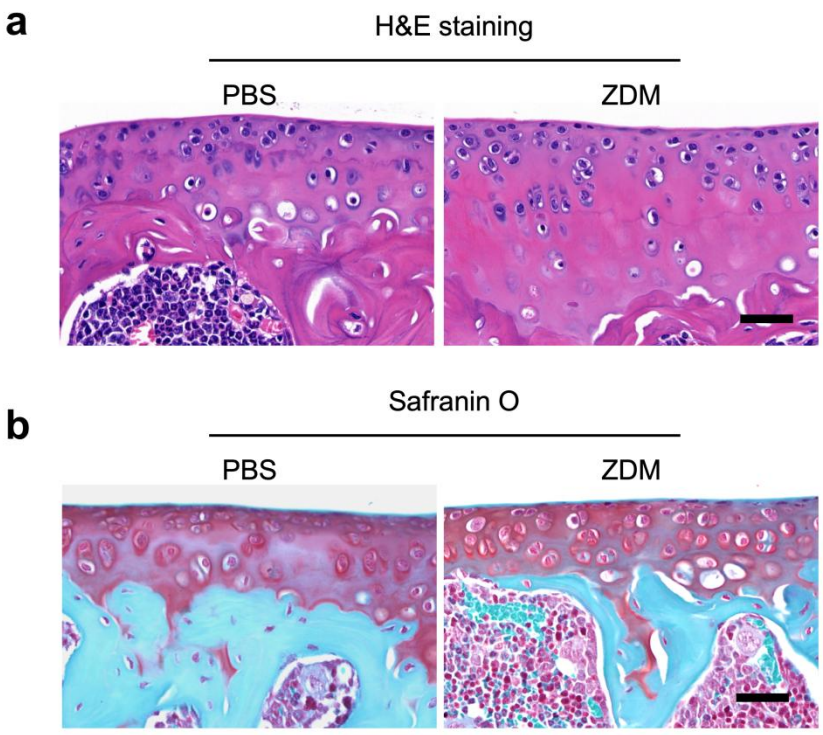

Supplementary Fig. 15. Histological evaluation of articular cartilage after intra-articular ZDM treatment.

a, Representative H&E staining images of articular cartilage from mice treated with PBS or ZDM.

b, Representative Safranin O staining images of articular cartilage from mice treated with PBS or ZDM.

These results show no obvious histopathological abnormalities in articular cartilage following intra-articular administration of ZDM. Scale bars, 100 μm.

`

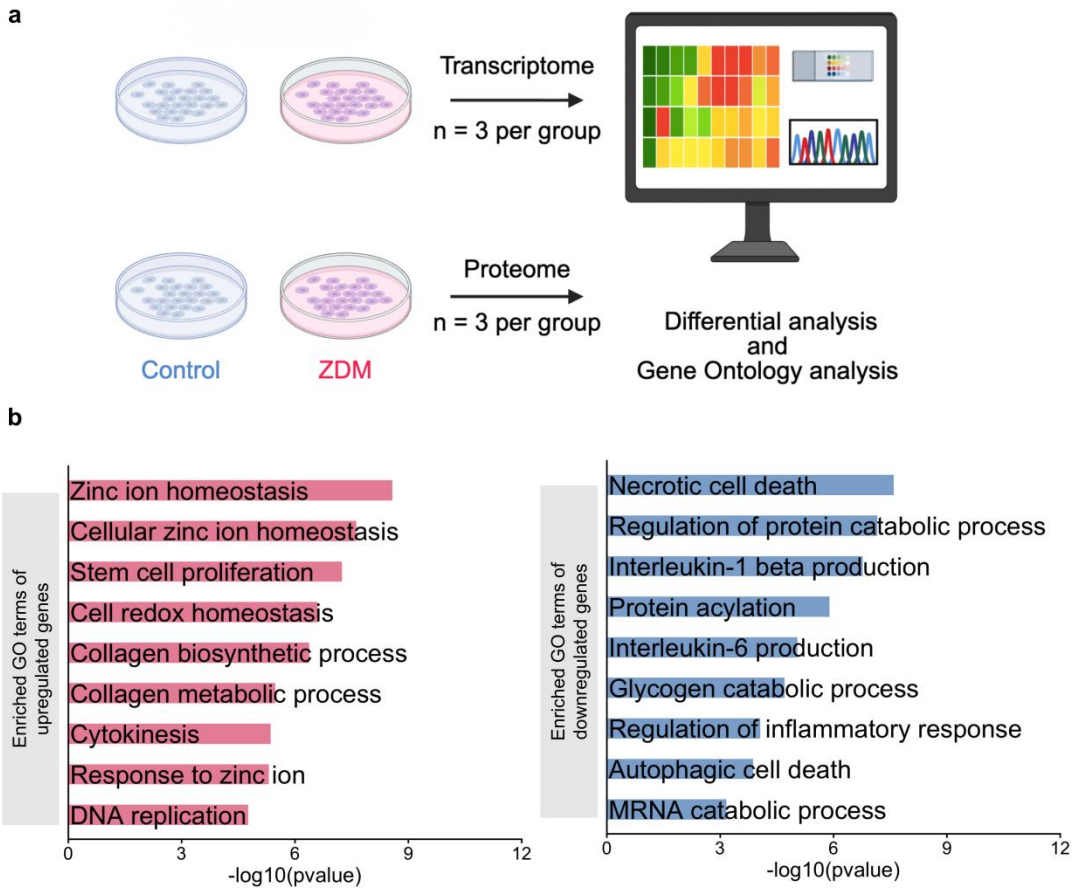

Supplementary Fig. 16. Experimental design and transcriptomic enrichment analysis of ZDM-treated cells.

a, Schematic illustration of the experimental design for transcriptomic and proteomic profiling treated with vehicle (Control) or ZDM (n = 3 per group). Differential expression and Gene Ontology (GO) analyses were subsequently performed.

b, GO enrichment analysis of upregulated and downregulated differentially expressed genes in ZDM-treated cells relative to control cells. Upregulated genes were enriched in pathways related to zinc ion homeostasis, cellular redox homeostasis, stem cell proliferation, collagen biosynthetic/metabolic processes, response to zinc ion and DNA replication, whereas downregulated genes were enriched in pathways related to necrotic cell death, regulation of protein catabolic process, interleukin-1 beta production, interleukin-6 production, regulation of inflammatory response, autophagic cell death and mRNA catabolic process.

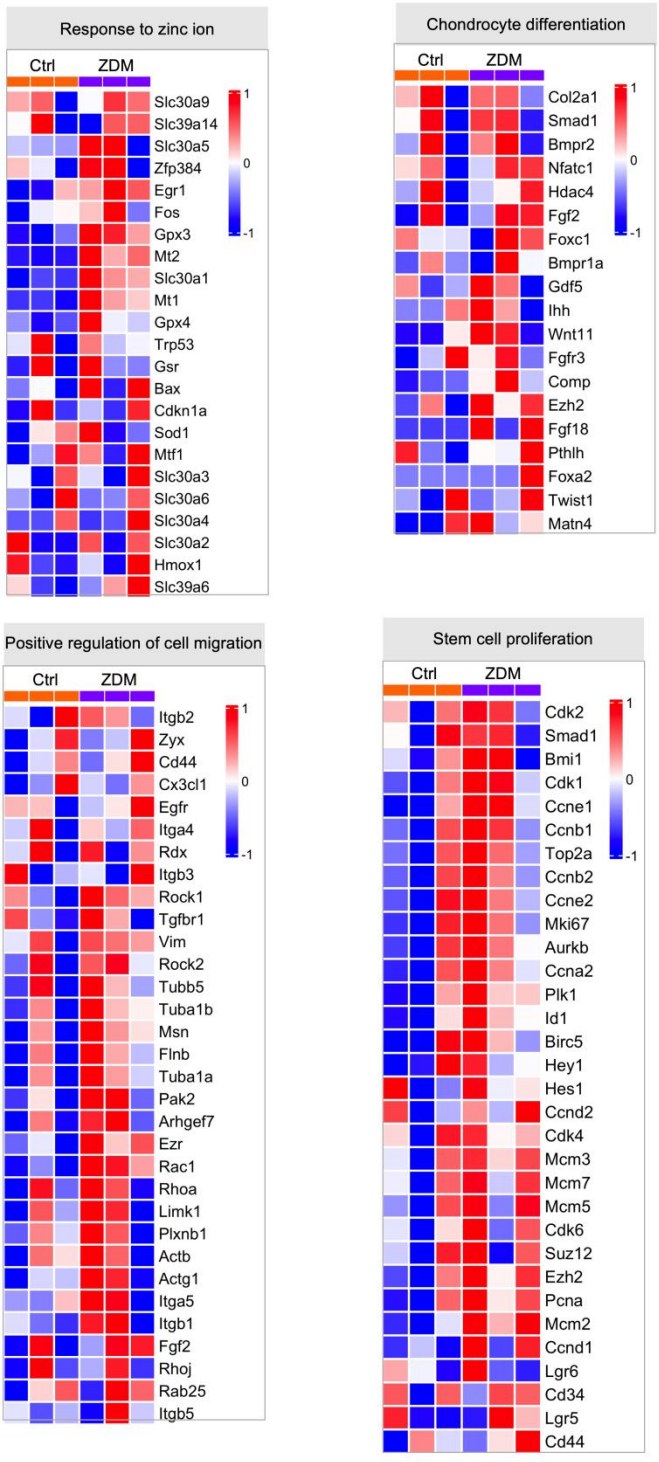

Supplementary Fig. 17. Heatmaps of representative transcriptomic changes induced by ZDM.

Heatmaps showing the expression of representative genes associated with response to zinc ion, chondrocyte differentiation, positive regulation of cell migration and stem cell proliferation in control (Ctrl) and ZDM-treated cells. Color scale represents normalized relative expression levels.

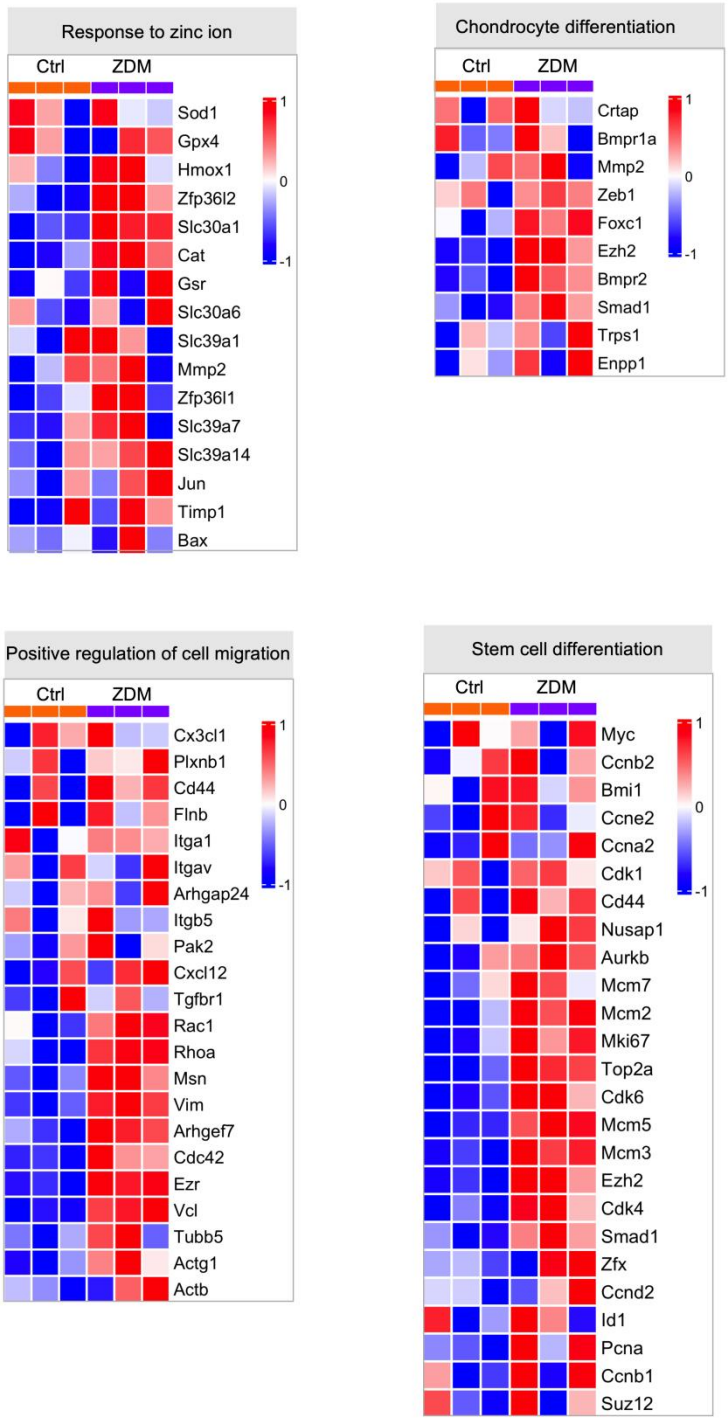

Supplementary Fig. 18. Heatmaps of representative proteomic changes induced by ZDM.

Heatmaps showing the expression of representative proteins associated with response to zinc ion, chondrocyte differentiation, positive regulation of cell migration and stem cell differentiation in control (Ctrl) and ZDM-treated cells. Color scale represents normalized relative expression levels.

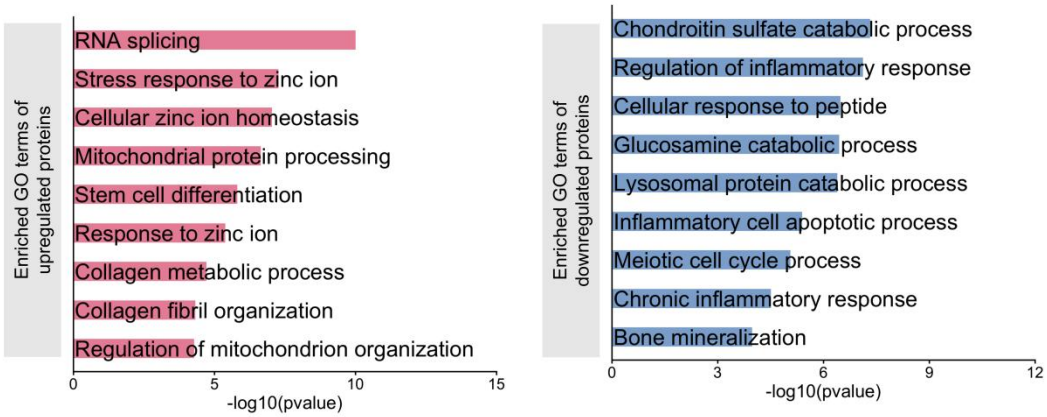

Supplementary Fig. 19. Proteomic Gene Ontology enrichment analysis of ZDM-treated cells.

Gene Ontology (GO) enrichment analysis of upregulated and downregulated differentially expressed proteins in ZDM-treated cells relative to control cells. Upregulated proteins were enriched in pathways related to RNA splicing, stress response to zinc ion, cellular zinc ion homeostasis, mitochondrial protein processing, stem cell differentiation, collagen metabolic process, collagen fibril organization and regulation of mitochondrion organization. Downregulated proteins were enriched in pathways related to chondroitin sulfate catabolic process, regulation of inflammatory response, cellular response to peptide, glucosamine catabolic process, lysosomal protein catabolic process, inflammatory cell apoptotic process, chronic inflammatory response and bone mineralization.

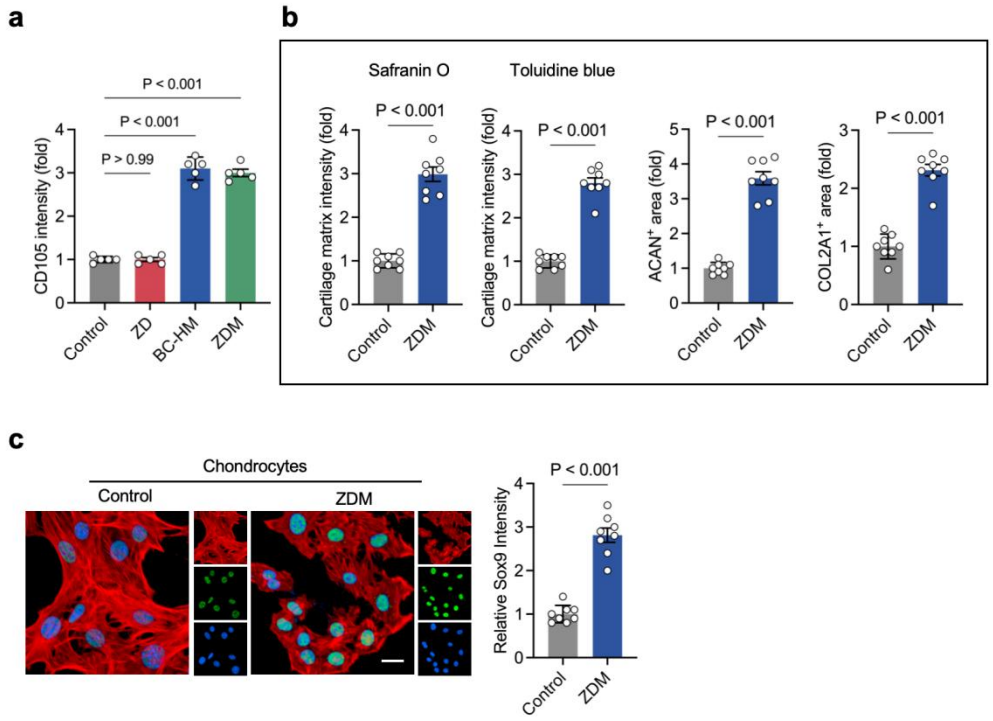

Supplementary Fig. 20. Quantification of MSC-associated stromal-cell accumulation and chondrogenic responses induced by ZDM.

a, Quantification of CD105 fluorescence intensity in joint sections from the indicated groups, showing enhanced accumulation of CD105-positive stromal/MSC-associated cells after treatment with MC-HM or ZDM.

b, Quantification of Safranin O staining intensity, toluidine blue staining intensity, ACAN-positive area and COL2A1-positive area in chondrogenic pellets from the indicated groups.

c, Representative immunofluorescence images and quantification of SOX9 expression in chondrocytes treated with vehicle (Control) or ZDM.

Data are presented as mean ± s.d. (**a–c**). Each dot represents one biologically independent sample. P values were determined using one-way ANOVA followed by Tukey's multiple-comparison test (**a**) or two-sided unpaired Student's t-test (**b,c**). Scale bars, 10 μm (**c**).

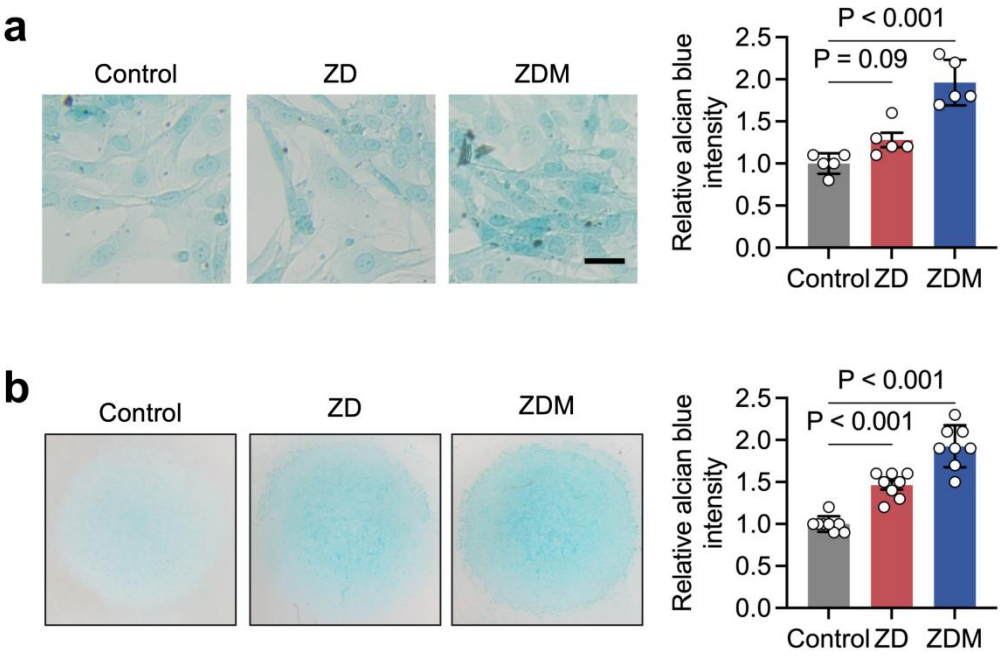

Supplementary Fig. 21. Additional validation of chondrogenic responses induced by ZD and ZDM.

a, Representative Alcian blue staining images and quantification of staining intensity in chondrocytes treated with Control, ZD or ZDM. Scale bars, 20 μm.

b, Representative Alcian blue staining images and quantification of staining intensity in chondrogenic pellets from the indicated groups.

Data are presented as mean ± s.d. (**a,b**). Each dot represents one biologically independent sample. P values were determined using one-way ANOVA followed by Tukey's multiple-comparison test.

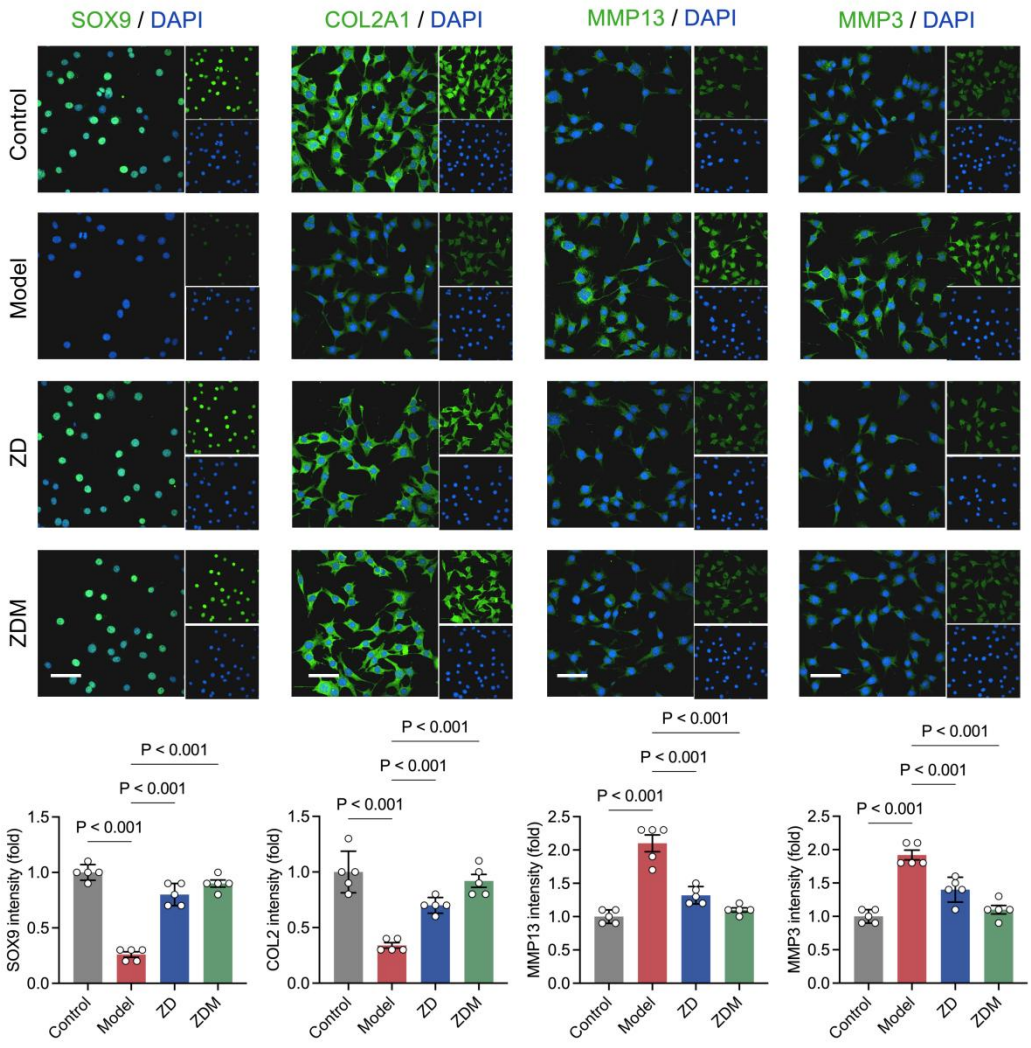

Supplementary Fig. 22. Additional validation of chondrogenic marker changes in the in vitro model after ZD or ZDM treatment.

Representative immunofluorescence images and quantification of SOX9, COL2A1, MMP13 and MMP3 expression in cells from the indicated groups (Control, Model, ZD and ZDM). Nuclei were counterstained with DAPI.

Data are presented as mean ± s.d. Each dot represents one biologically independent sample. P values were determined using one-way ANOVA followed by Tukey's multiple-comparison test. Scale bars, 10 μm.

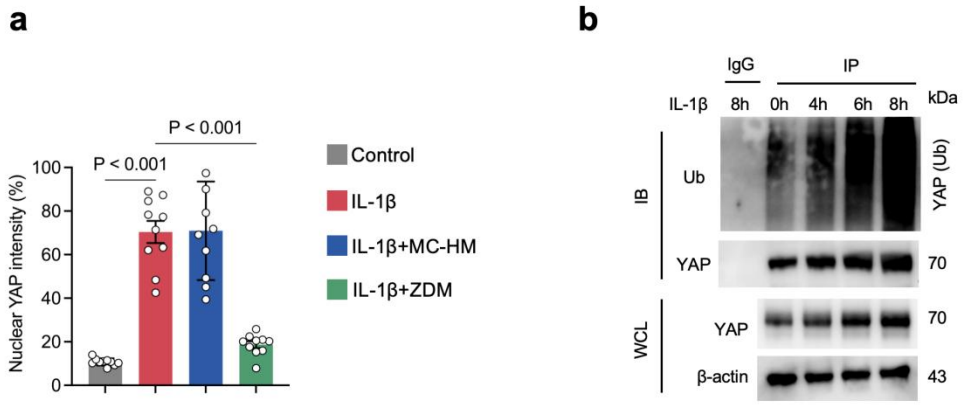

Supplementary Fig. 23. ZDM regulates YAP nuclear localization.

a, Quantification of nuclear YAP intensity in cells treated with control, IL-1β, IL-1β + MC-HM or IL-1β + ZDM.

b, Immunoprecipitation and western blot analysis of YAP ubiquitination after IL-1β treatment for the indicated times. Whole-cell lysates were used to detect total YAP and β-actin. Data are shown as mean ± s.d.; each dot represents an independent sample.

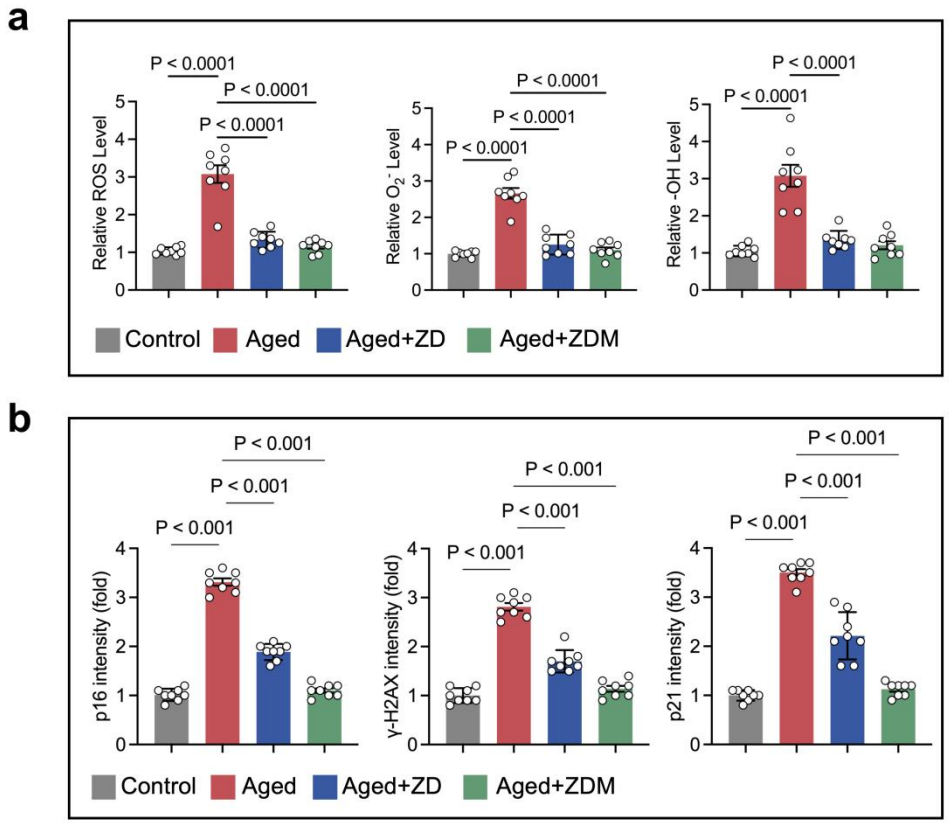

Supplementary Fig. 24. Quantification of oxidative stress and senescence markers.

a, Quantification of oxidative stress, including ROS, $O_2^{\bullet-}$ and ·OH levels, in control, aged, aged + ZD and aged + ZDM groups.

b, Quantification of senescence-associated markers, including p16 intensity, γ-H2AX intensity and p21 intensity, in the four groups. Data are shown as mean ± s.d.; each dot represents an independent sample. Statistical significance was assessed by one-way ANOVA with Tukey's test.

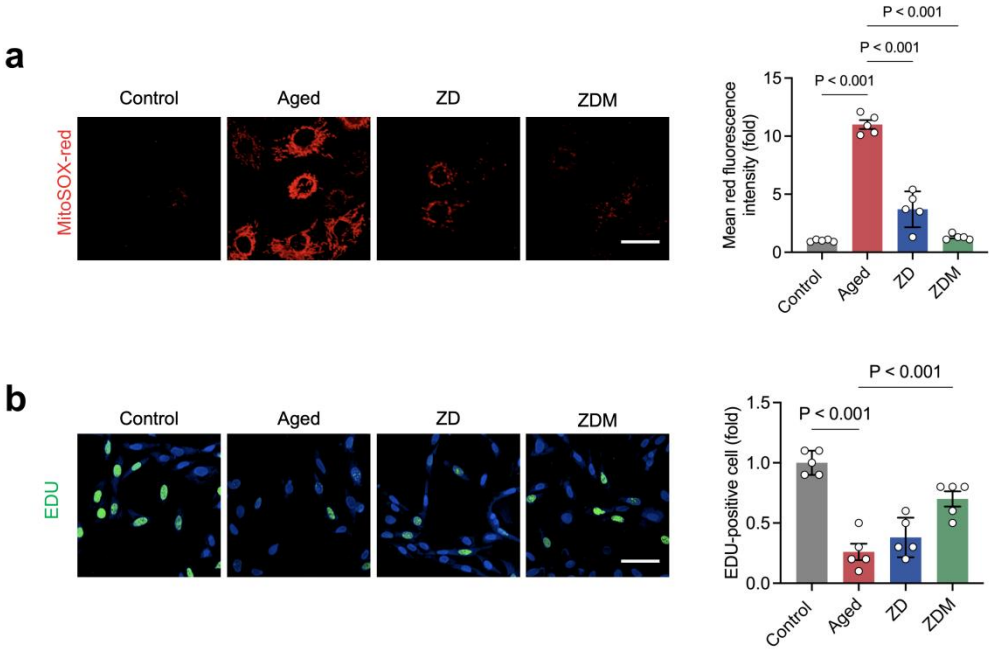

Supplementary Fig. 25. ZDM attenuates mitochondrial oxidative stress and restores cell proliferation.

a, Representative MitoSOX-red fluorescence images and quantification of mitochondrial ROS levels in control, aged, aged+ZD-treated and aged+ZDM-treated cells. Scale bars, 10 μm.

b, Representative EdU staining images and quantification of EdU-positive cells in the four groups. Data are shown as mean ± s.d.; each dot represents an independent sample. Statistical significance was assessed by one-way ANOVA with Tukey's test. Scale bars, 10 μm.

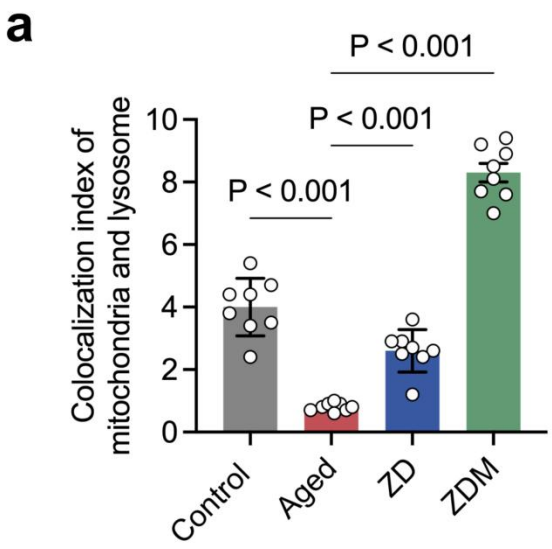

Supplementary Fig. 26. Quantification analysis of mitochondrial–lysosomal colocalization. Quantification of the mitochondria–lysosome colocalisation index in young control, aged, aged + ZD and aged + ZDM MSCs corresponding to Fig. 6f. Data are presented as mean ± s.d. Each dot represents one independent donor- or mouse-derived cell preparation. Statistical significance was determined using one-way ANOVA followed by Tukey's multiple-comparisons test.

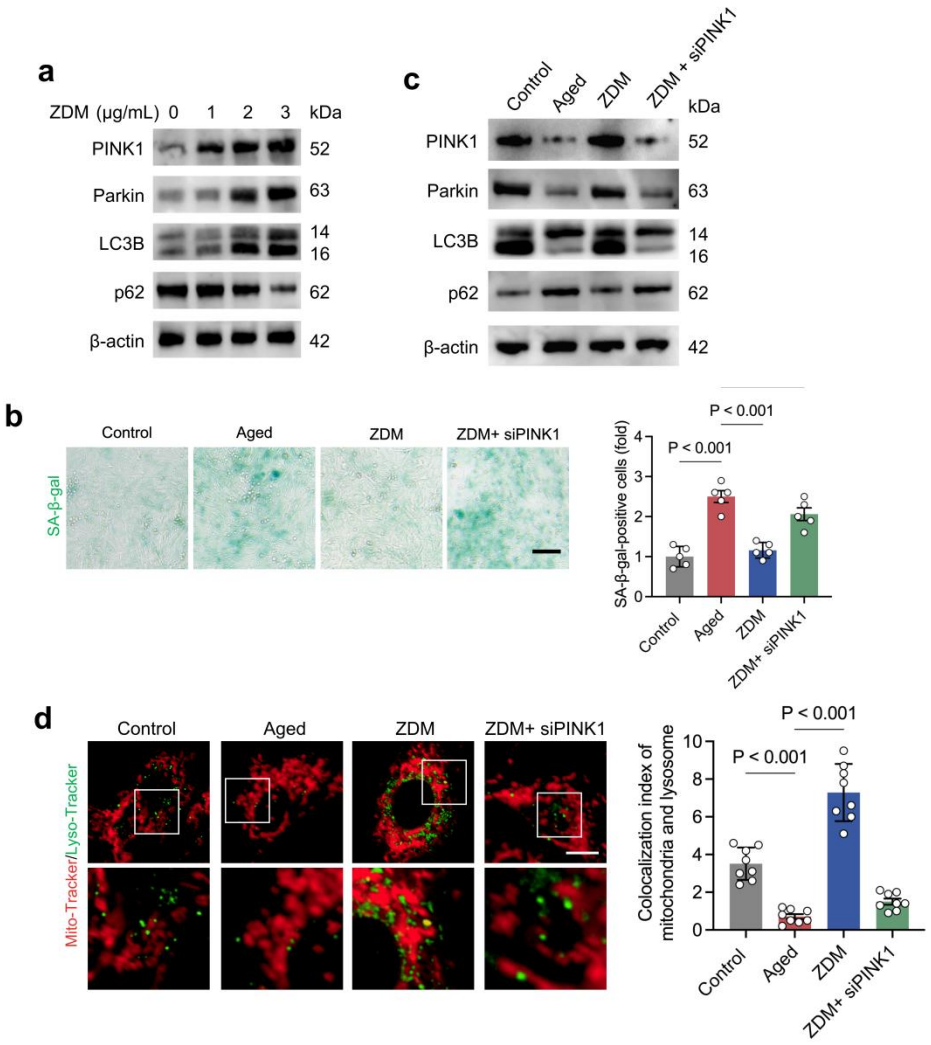

Supplementary Fig. 27. PINK1 contributes to the pro-mitophagy and anti-senescence effects of ZDM.

a, Western blot analysis of PINK1, Parkin, LC3B and p62 in aged cells treated with increasing concentrations of ZDM.

b, Representative SA-β-gal staining and quantification of SA-β-gal-positive cells in control, aged, aged+ZDM-treated and aged+ZDM + siPINK1 cells.

c, Western blot analysis of PINK1, Parkin, LC3B and p62 in control, aged, aged+ZDM-treated and aged+ZDM + siPINK1 cells.

d, Representative super-resolution images and quantification of mitochondrial–lysosomal colocalization in the indicated groups. Data are shown as mean ± s.d.; each dot represents an independent sample. Statistical significance was assessed by one-way ANOVA with Tukey's test.

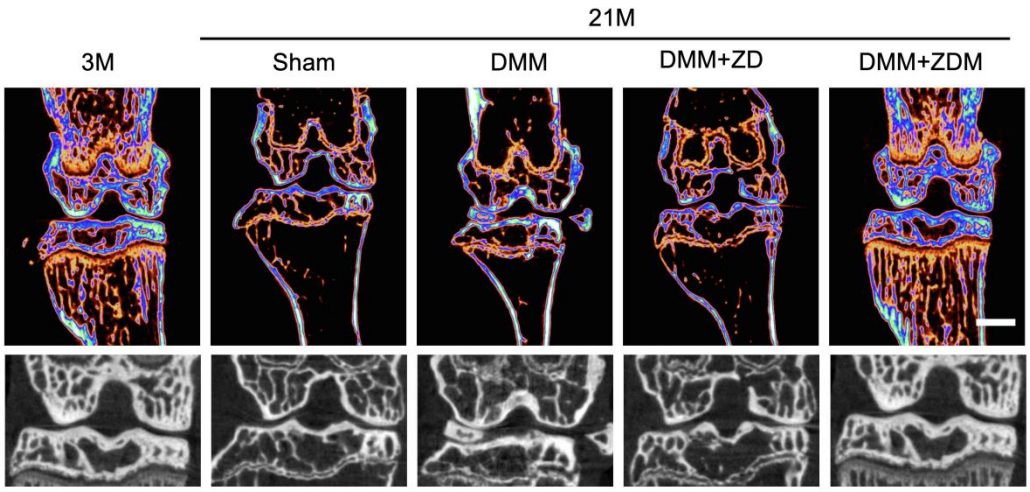

Supplementary Fig. 28. Pseudo-coloured micro-CT cross-sectional images of mouse knee joints.

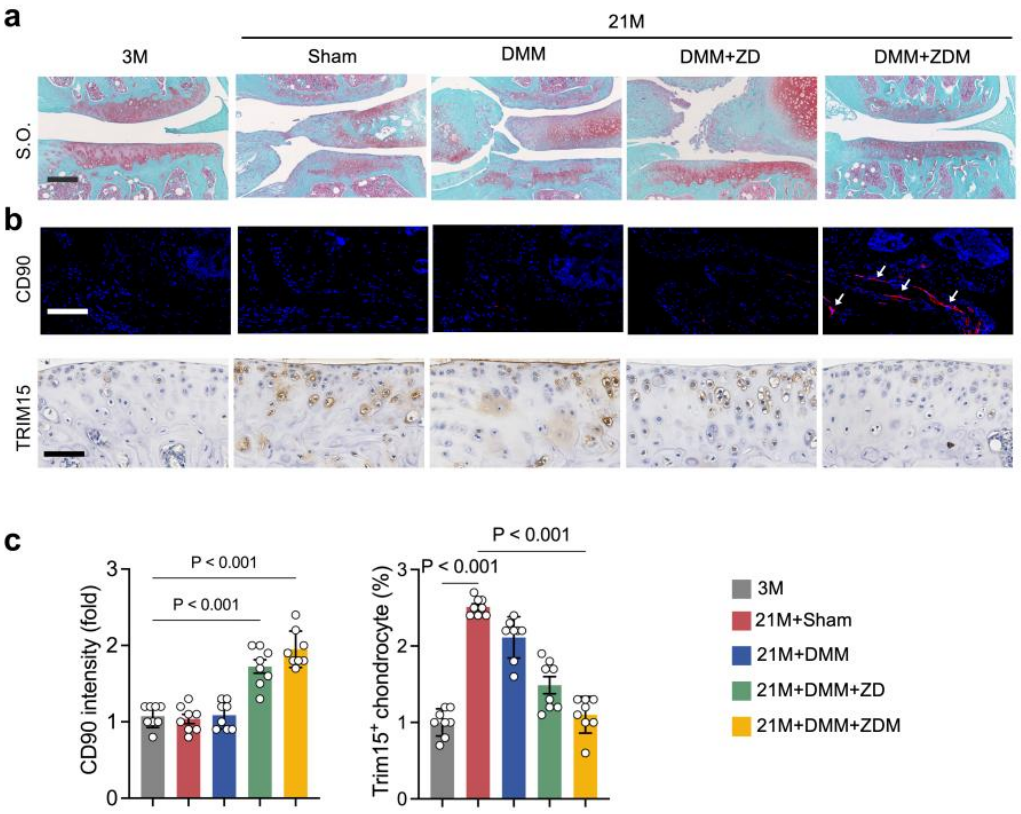

Supplementary Fig. 29. ZDM preserves cartilage matrix, promotes MSC-associated cell accumulation and reduces TRIM15 expression in aged DMM mice.

a, Representative Safranin O staining images of knee joints from 3-month-old mice (3M) and 21-month-old (21M) mice in the Sham, DMM, DMM + ZD and DMM + ZDM groups.

b, Representative immunofluorescence staining images of CD90 and immunohistochemical staining images of TRIM15 in knee joint sections from the indicated groups. Arrows indicate representative CD90-positive stromal/MSC-like cells in the joint region.

c, Quantification of CD90 fluorescence intensity and the percentage of TRIM15-positive chondrocytes in the indicated groups.

Data are presented as mean ± s.d. (**c**). Each dot represents one biologically independent mouse joint. P values were determined using one-way ANOVA followed by Tukey's multiple-comparison test. Scale bars, 100 μm.

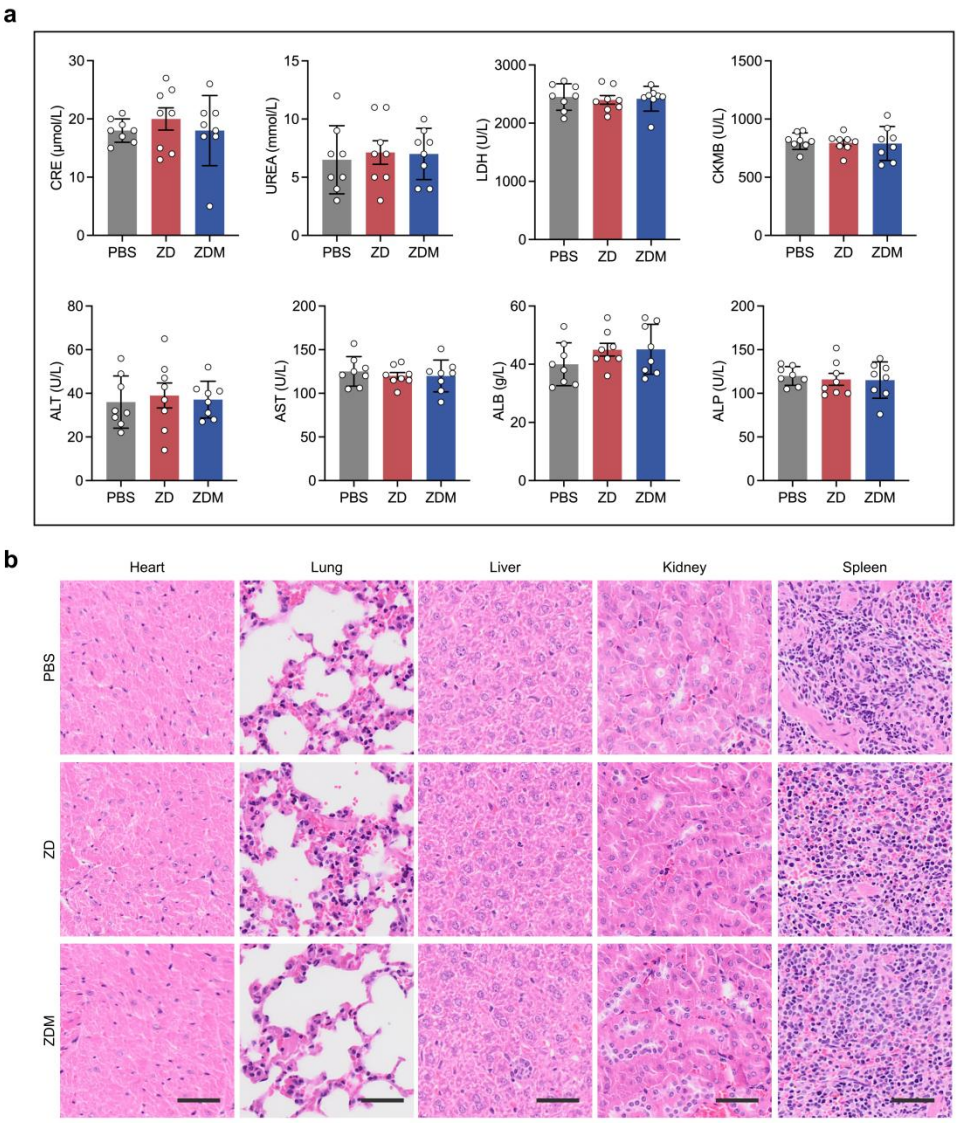

Supplementary Fig. 30. In vivo biosafety evaluation of intra-articular ZD and ZDM administration.

a, Serum biochemical analysis of mice treated with PBS, ZD or ZDM, including CRE, UREA, LDH, CKMB, ALT, AST, ALB and ALP. No significant abnormalities were observed among groups.

b, Representative H&E staining images of major organs, including the heart, lung, liver, kidney and spleen, from mice treated with PBS, ZD or ZDM. No obvious histopathological abnormalities were observed after treatment.

Data are presented as mean ± s.d.(**a**). Each dot represents one biologically independent animal. Scale bars, 100 μm.

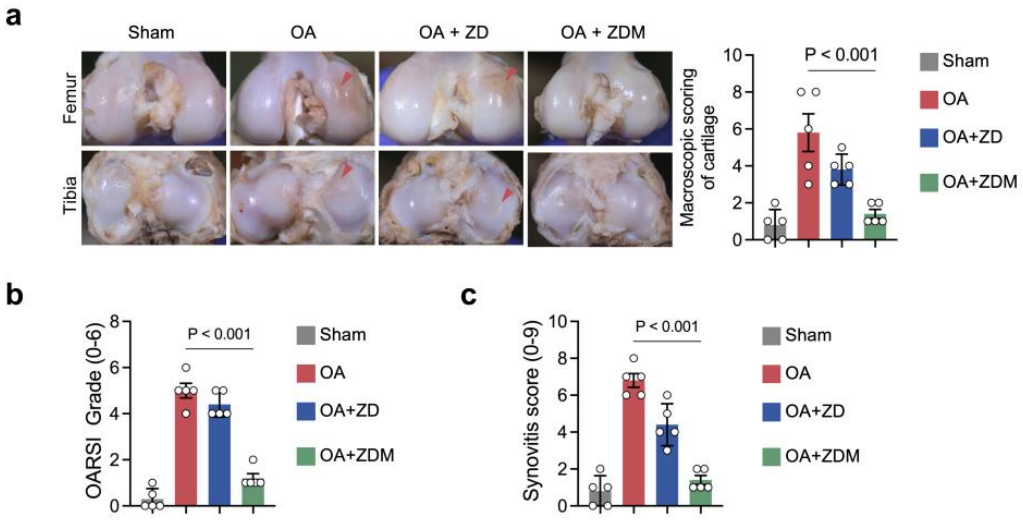

Supplementary Fig. 31. Gross and semi-quantitative evaluation of cartilage degeneration in beagle dog joints after ZD or ZDM treatment.

a, Representative gross photographs of femoral condyles and tibial plateaus from Sham, OA, OA + ZD and OA + ZDM beagle dogs, with quantification of macroscopic cartilage scores. Red arrowheads indicate representative cartilage surface erosion or defect regions.

b, Quantification of histological cartilage degeneration using the OARSI grade scoring system in the indicated groups.

c, Quantification of synovitis scores in the indicated groups.

Ordinal data are presented as median with interquartile range. Each dot represents one biologically independent beagle dog. Statistical significance was determined using the Kruskal–Wallis test followed by Dunn's multiple-comparison test (**a–c**).

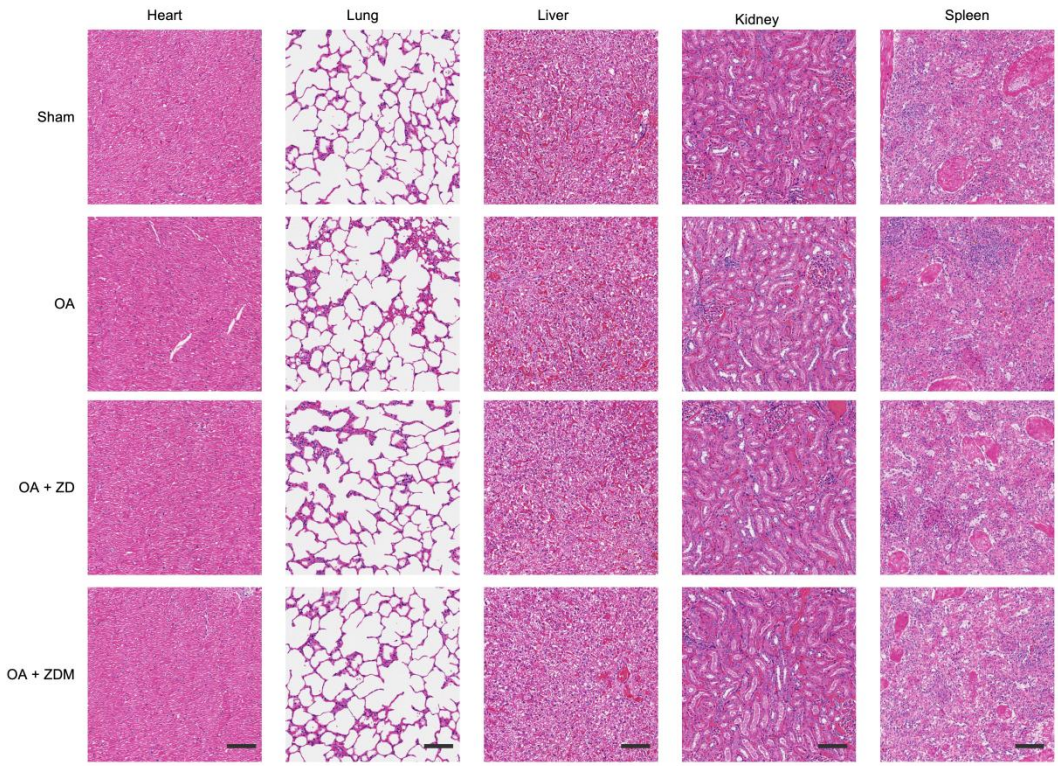

Supplementary Fig. 32. Histological evaluation of major organs in beagle dogs after ZD or ZDM treatment.

Representative H&E staining images of major organs, including the heart, lung, liver, kidney and spleen, from Sham, OA, OA + ZD and OA + ZDM beagle dogs. No obvious histopathological abnormalities were observed in the major organs after intra-articular administration of ZD or ZDM, indicating no overt histopathological toxicity in major organs. Scale bars, 100 μm.

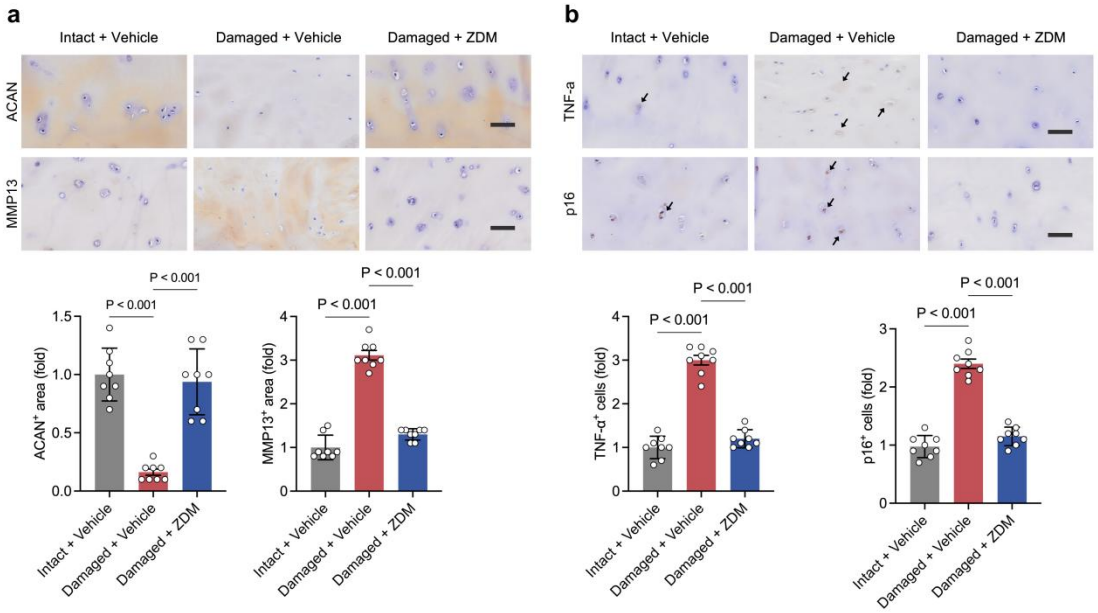

Supplementary Fig. 33. ZDM restores matrix homeostasis and suppresses inflammatory and senescence-associated signals in damaged human cartilage explants.

a, Representative immunohistochemical staining images and quantification of ACAN and MMP13 in intact human cartilage explants treated with vehicle, damaged cartilage explants treated with vehicle, and damaged cartilage explants treated with ZDM. ZDM restored ACAN expression and reduced MMP13 expression in damaged cartilage explants.

b, Representative immunohistochemical staining images and quantification of TNF-α and p16 in the indicated human cartilage explant groups. Arrows indicate representative positive cells. ZDM reduced inflammatory and senescence-associated signals in damaged cartilage explants.

Data are presented as mean ± s.d. (**a,b**). Each dot represents one biologically independent human cartilage specimen. Scale bars, 100 μm.

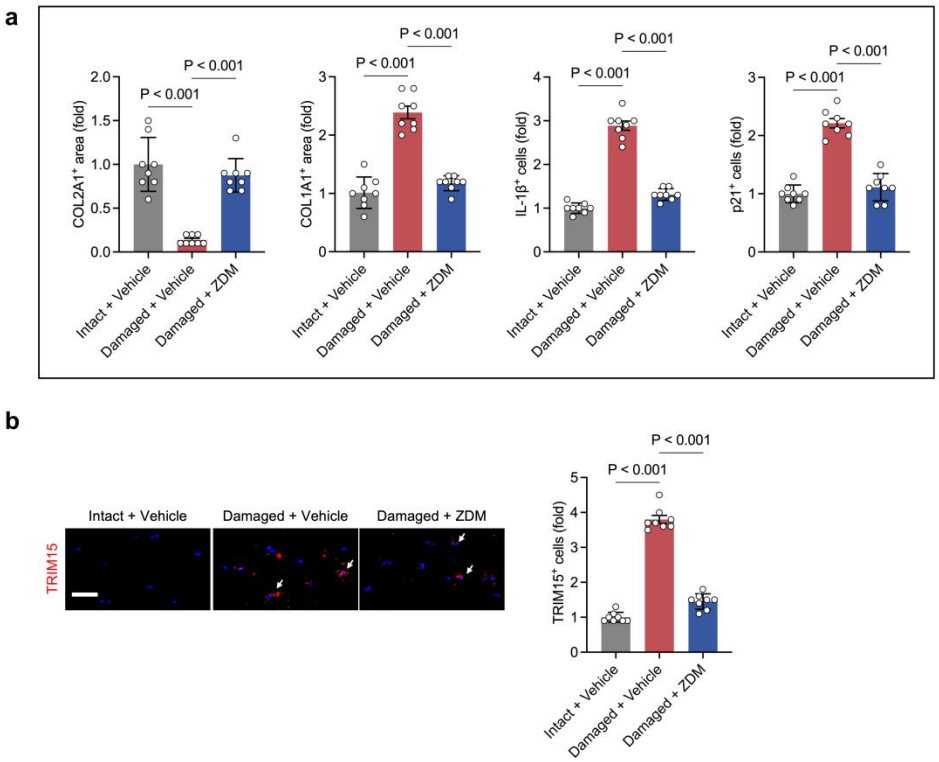

Supplementary Fig. 34. ZDM restores anabolic matrix markers and suppresses inflammatory, senescence-associated and TRIM15 signals in damaged human cartilage explants.

a, Quantification of COL2A1-positive area, COL1A1-positive area, IL-1β-positive cells and p21-positive cells in intact human cartilage explants treated with vehicle, damaged cartilage explants treated with vehicle, and damaged cartilage explants treated with ZDM. ZDM restored COL2A1 expression and reduced COL1A1, IL-1β and p21 signals in damaged cartilage explants.

b, Representative immunofluorescence images and quantification of TRIM15-positive cells in the indicated human cartilage explant groups. Arrows indicate representative TRIM15-positive cells.

Data are presented as mean ± s.d. (**a,b**). Each dot represents one biologically independent human cartilage specimen. Scale bars, 100 μm.

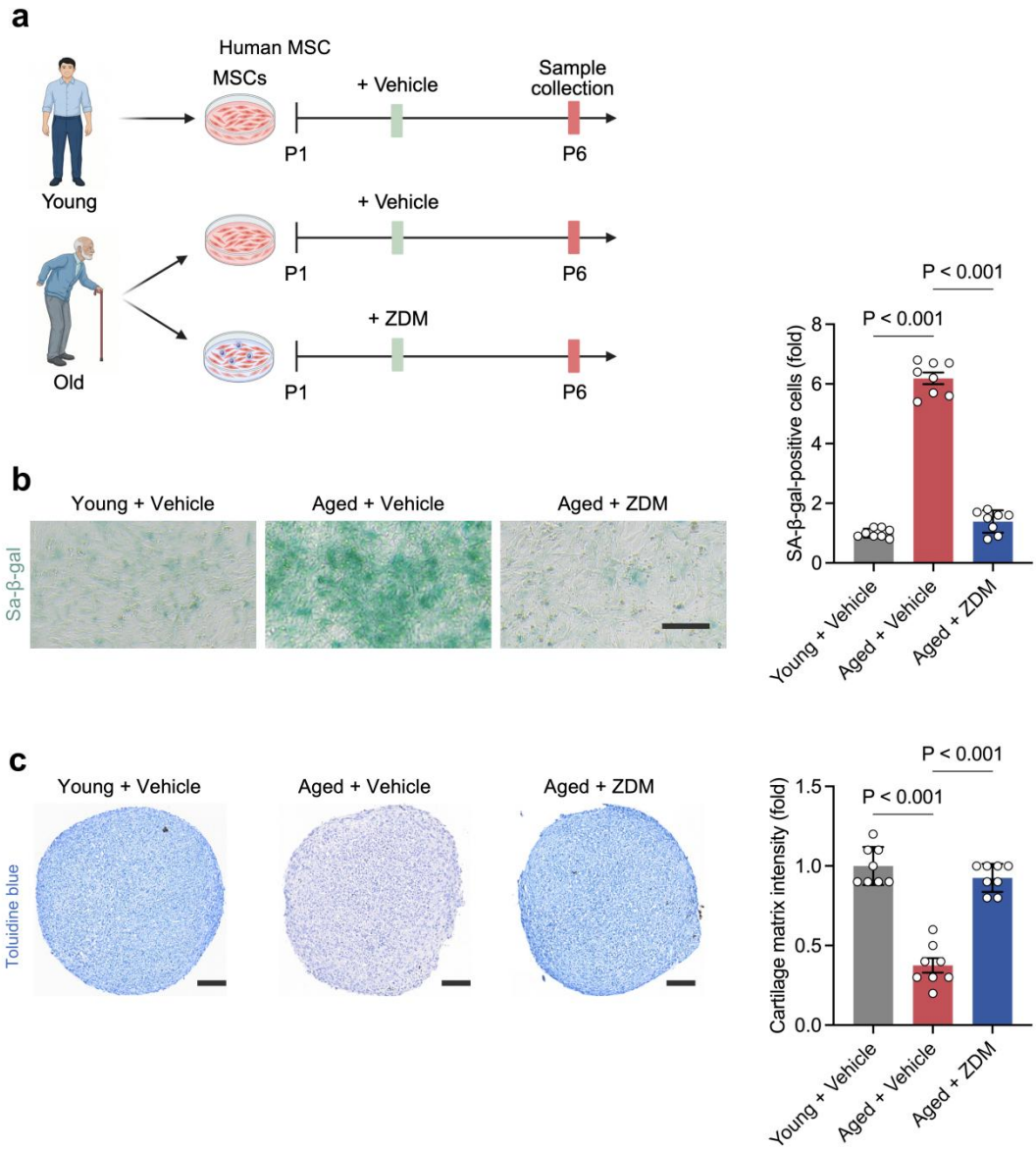

Supplementary Fig. 35. ZDM reduces senescence and improves chondrogenic matrix formation in aged human MSCs.

a, Experimental design. Human MSCs from young and aged donors were expanded from P1 to P6 with vehicle or ZDM treatment.

b, Representative SA-β-gal staining and quantification of SA-β-gal-positive cells. Scale bars, 20 μm.

c, Toluidine blue staining and quantification of chondrogenic pellets. ZDM restored glycosaminoglycan-rich matrix deposition in aged MSCs. Scale bars, 20 μm

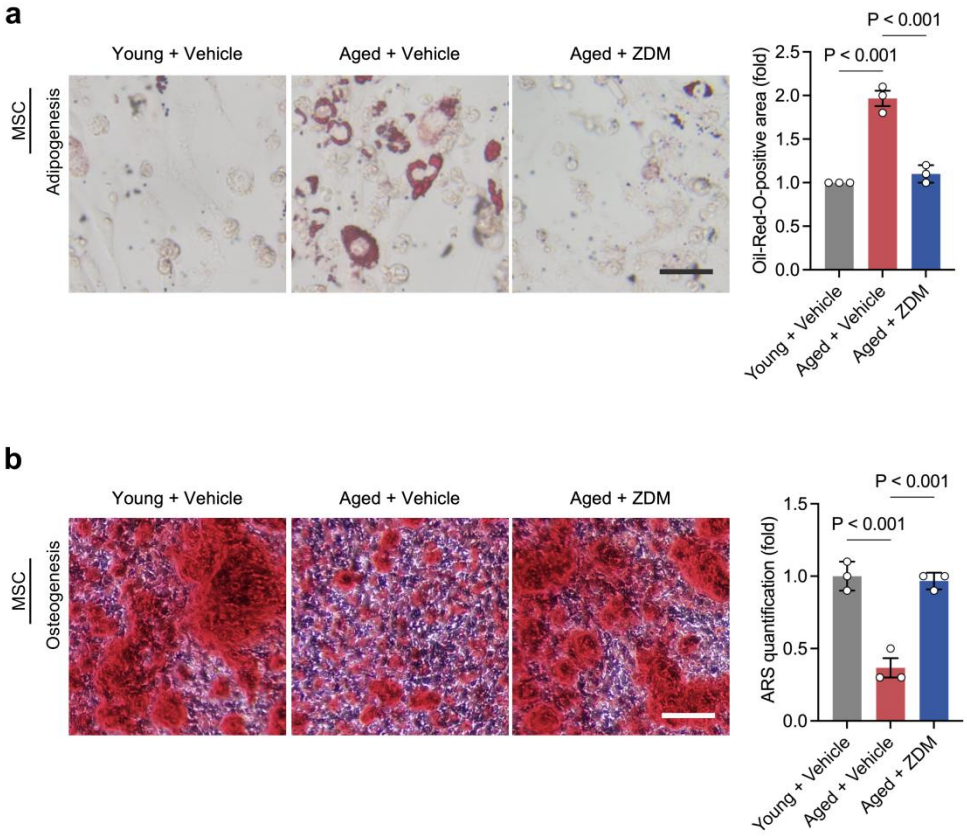

Supplementary Fig. 36. Adipogenic and osteogenic differentiation of human MSCs after ZDM treatment.

a, Representative Oil Red O staining and quantification of Oil Red O-positive area in young vehicle-treated, aged vehicle-treated and aged ZDM-treated MSCs after adipogenic induction. Scale bars, 20 μm.

b, Representative Alizarin Red S staining and quantification of mineralized matrix deposition in the three groups after osteogenic induction. Data are shown as mean ± s.d.; each dot represents an independent replicate. Statistical significance was assessed by one-way ANOVA with Tukey's test. Scale bars, 20 μm.

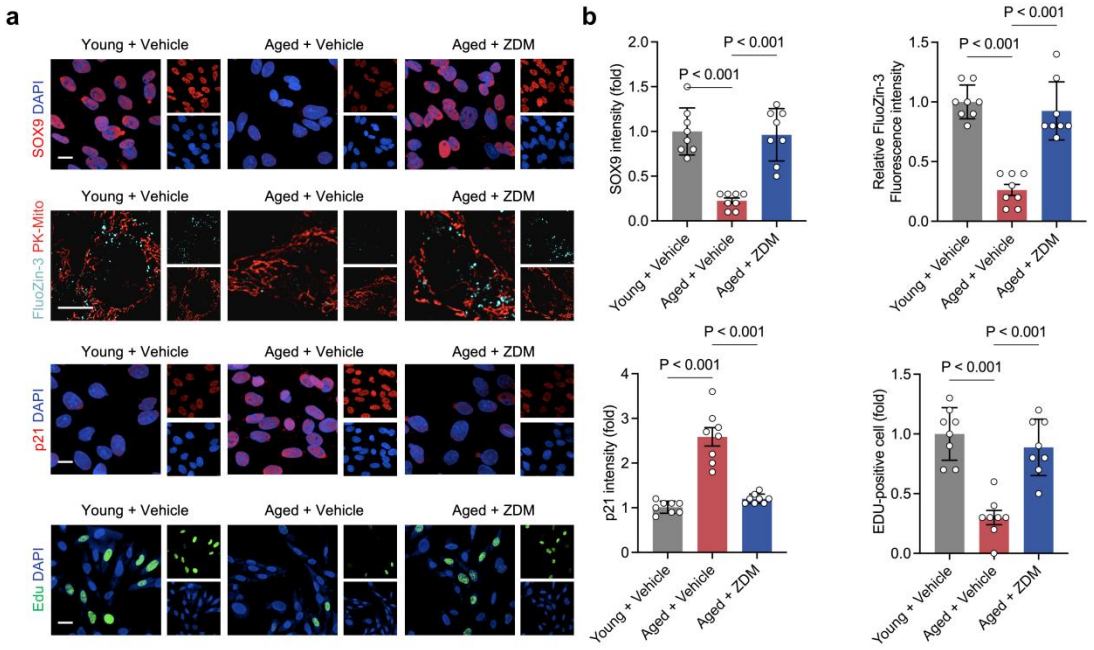

Supplementary Fig. 37. ZDM promotes rejuvenation of aged human MSCs.

a, Representative fluorescence images of SOX9, FluoZin-3/PK-Mito, p21 and EdU staining in young vehicle-treated, aged vehicle-treated and aged ZDM-treated MSCs. Nuclei were counterstained with DAPI. Scale bars, 10 μm.

b, Quantification of SOX9 intensity, FluoZin-3 fluorescence intensity, p21 intensity and Edu-positive cells in the three groups. Data are shown as mean ± s.d.; each dot represents an independent replicate. Statistical significance was assessed by one-way ANOVA with Tukey's test.

Supplementary Table 1. Characteristics of human articular cartilage and MSC donors.

Sample	Age	KL	Extraction site
Young-1	37	2	Right tibial plateau
Young-2	41	2	Left tibial plateau
Young-3	39	2	Right tibial plateau
Young-4	45	1	Right tibial plateau
Young-5	34	2	Right tibial plateau
Young-6	36	3	Left femoral condyles
Young-7	42	2	Right tibial plateau
Young-8	43	2	Right tibial plateau
Old-9	71	4	Right tibial plateau
Old-10	81	3	Right femoral condyles
Old-11	85	4	Right tibial plateau
Old-12	75	3	Right tibial plateau
Old-13	89	3	Right femoral condyles
Old-14	90	3	Right tibial plateau
Old-15	78	4	Right tibial plateau
Old-16	86	4	Right femoral condyles
Young-MSC-1	35	NA	MSC
Young-MSC-2	42	NA	MSC
Young-MSC-3	36	NA	MSC
Young-MSC-4	39	NA	MSC
Young-MSC-5	45	NA	MSC
Young-MSC-6	41	NA	MSC
Young-MSC-7	34	NA	MSC
Young-MSC-8	43	NA	MSC
MSC-9	78	NA	MSC
MSC-10	91	NA	MSC
MSC-11	85	NA	MSC
MSC-12	87	NA	MSC
MSC-13	79	NA	MSC
MSC-14	83	NA	MSC
MSC-15	86	NA	MSC
MSC-16	76	NA	MSC

Supplementary Table 2. List of primary and secondary antibodies used in the study.

Antibodies	Source	Identifier	Dilution/Application
Rabbit anti-TRIM15/RNF93	Abcam	ab229273	WB (1:1,000); IHC/IF (1:200)
Rabbit anti-COL2/COL2A1	Boster Biological Technology	BA0533	WB (1:1,000); IHC (1:200); IF (1:200)
Mouse anti-SOX9	Proteintech	67439-1-Ig	WB (1:1,000); IF (1:200)
Rabbit anti-MMP13	Proteintech	18165-1-AP	WB (1:1,000); IHC (1:200); IF (1:200)
Rabbit anti-p53	Proteintech	10442-1-AP	WB (1:1,000)
Rabbit anti-p21	Proteintech	10355-1-AP	WB (1:1,000); IHC (1:200); IF (1:200)
Rabbit anti-p16	Proteintech	10883-1-AP	WB (1:1,000); IHC (1:200); IF (1:200)
Rabbit anti-gamma-H2AX	Proteintech	83307-2-RR	IF (1:200)
Rabbit anti-ITGA2	Proteintech	30703-1-AP	WB (1:1,000); IF (1:200); IP
Rabbit anti-COL1/COL1A1	Proteintech	14695-1-AP	IHC (1:200); IF (1:200); IP
Rabbit anti-Na+/K+-ATPase	Proteintech	14418-1-AP	WB (1:1,000)
Rabbit anti-E-cadherin	Proteintech	20874-1-AP	WB (1:1,000); IF (1:200)
Rabbit anti-N-cadherin	Proteintech	22018-1-AP	WB (1:1,000); IF (1:200)
Rabbit anti-CD44	Proteintech	15675-1-AP	WB (1:1,000); IF (1:200)
Rabbit anti-Integrin beta1	Proteintech	12594-1-AP	WB (1:1,000)
Mouse anti-Integrin alpha3	Proteintech	66070-1-Ig	WB (1:1,000)
Rabbit anti-CD105	Proteintech	10862-1-AP	IF (1:200)
Rabbit anti-ACAN	Proteintech	13880-1-AP	IHC (1:200); IF (1:200)
Rabbit anti-YAP	Proteintech	13584-1-AP	WB (1:1,000); IF (1:200); IP
Rabbit anti-PINK1	Proteintech	23274-1-AP	WB (1:1,000); IF (1:200)
Rabbit anti-Parkin	Proteintech	14060-1-AP	WB (1:1,000)
Rabbit anti-LC3B	Proteintech	14600-1-AP	WB (1:1,000)
Rabbit anti-p62/SQSTM1	Proteintech	18420-1-AP	WB (1:1,000)
Rabbit anti-SIRT1	Proteintech	13161-1-AP	WB (1:1,000)
Mouse anti-PGC1alpha	Proteintech	66369-1-Ig	WB (1:1,000)

Antibodies	Source	Identifier	Dilution/Application
Rabbit anti-TFAM	Proteintech	22586-1-AP	WB (1:1,000)
Rabbit anti-MMP3	Proteintech	17873-1-AP	IF (1:200)
Rabbit anti-IL-1beta	Proteintech	16806-1-AP	IHC (1:200)
Rabbit anti-TNF-alpha	Proteintech	17590-1-AP	IHC (1:200)
Mouse anti-beta-actin	Proteintech	66009-1-Ig	WB (1:1,000)
Anti-HA magnetic beads	Thermo Scientific	88836	IP, as recommended by manufacturer
Anti-FLAG magnetic beads	Thermo Scientific	A36797	IP, as recommended by manufacturer

Supplementary Table 3. List of primers.

Target	For qPCR detection	Primer sequence
Pink1	FORWARD	CAATGCCGCTGTGTATGAA
	REVERSE	CAAAGGGAAAGGTGGGAGT
Prkn	FORWARD	CCAACCTCAGACAAGGACA
	REVERSE	GAGGCACCAGATGACAGAG
Tfam	FORWARD	CATCCCCTCGTCTATCAGTC
	REVERSE	GCATCTGGGTGTTTAGCTTT
Ppargc1a	FORWARD	CTCAAGCCAAACCAACAAC
	REVERSE	CAGTTCCAGAGAGTTCCACA
Sirt1	FORWARD	GGTTCATTTATCAGAGTTGCC
	REVERSE	TGTTGTTTGTTGCTTGGTCT
Cdkn1a	FORWARD	CAAAGTGTGCCGTTGTCTCT
	REVERSE	CAAAGTTCCACCGTTCTCG
Actb	FORWARD	TAAGGCCAACCGTGAAAAG
	REVERSE	GACCAGAGGCATACAGGGA

Supplementary Table 4. TRIM15-targeting DNAzyme oligonucleotides

Oligonucleotide	Species	Target	Sequence	Application
hTRIM15-Dz	Human	TRIM15	AATCACGGAGGCTAGCTA CAACGACTTCTTGAC	TRIM15-targeting DNAzyme
mTrim15-Dz	Mouse	Trim15	GCCACTGTAGGCTAGCTA CAACGATGAGGAGGT	TRIM15-targeting DNAzyme
cfaTRIM15-Dz	Dog	TRIM15	GCTGCTGCAGGCTAGCTA CAACGATGAGGAGAC	TRIM15-targeting DNAzyme